Lattice polaron formation: Effects of nonscreened electron-phonon interaction

H. Fehske
Physikalisches Institut, Universität Bayreuth, 95440 Bayreuth, Germany

J. Loos
Institute of Physics, Czech Academy of Sciences, 16200 Prague, Czech Republic

G. Wellein
Regionales Rechenzentrum Erlangen, Universität Erlangen, 91058 Erlangen, Germany

(Received 11 November 1999)

We explore the quasiparticle properties of lattice polarons on the basis of a quite general electron-phonon Hamiltonian with a long-range displacement-type interaction. To treat the dynamical quantum phonons without significant loss of accuracy we adapt an exact Lanczos diagonalization method and compute various static and dynamical quantities, such as the electron-lattice correlation function, the polaron band dispersion, the effective polaron mass, the kinetic energy, the single-particle spectral function, and the optical conductivity, on finite one-dimensional lattices for a wide range of model parameters. We compare the results with those obtained for the standard Holstein model with short-range electron-phonon interaction only.

I. INTRODUCTION

The classical polaron problem[1] has received renewed attention on account of the observation of polaronic effects in several important classes of materials, including high-temperature cuprate superconductors and colossal magnetoresistance manganites.[2,3] Remarkably even the much simpler case of free electrons interacting with optical phonons in ionic crystals is still not completely understood. From a theoretical point of view the challenge is to describe the crossover from an only weakly dressed charge carrier to the strongly mass-enhanced, i.e., less mobile, polaronic quasiparticle with increasing electron-lattice coupling strength. Depending on the relative importance of the short- or long-range electron-phonon (EP) coupling, simplified models of the Holstein[4] or Fröhlich[5] type, respectively, have been studied over the last five decades. However, despite extensive analytical work, in the physically most interesting crossover regime, up to now, the only reliable results came from numerical studies, such as finite-cluster exact diagonalizations (ED),[6–11] quantum Monte Carlo (QMC) simulations,[12,13] density-matrix renormalization-group approaches,[14,15] and global-local[16] or variational methods.[17]

Recently the formation of small polarons was investigated by Alexandrov and Kornilovitch[18] applying a new path-integral Monte Carlo algorithm.[19,20] These authors introduced the following EP Hamiltonian:

$$\mathcal{H}=-t\sum_{\langle j,j'\rangle} c_{j'}^{\dagger}c_j+\omega_0\sum_l\left(b_l^{\dagger}b_l+\frac{1}{2}\right)$$

$$-\sum_{j,l} f_l(j)c_j^{\dagger}c_j x_0(b_l^{\dagger}+b_l). \tag{1}$$

Here $c_j^{[\dagger]}$ and $b_j^{[\dagger]}$ denote fermionic and bosonic annihilation [creation] operators, respectively. Restricting ourselves to the one-dimensional (1D) case, $\mathcal{H}$ describes an electron in a Wannier state on site j of an infinite chain which interacts with the vibrations of all ions of another chain via a ''density-displacement'' type long-range EP coupling

$$f_l(j)=\frac{\kappa}{(|l-j|^2+1)^{3/2}} \tag{2}$$

(cf. Fig. 1 of Ref. 18). The distance $|l-j|$ is measured in units of the lattice constant. In Eq. (1), $x_0=\sqrt{1/2M\omega_0}$, $\kappa x_0=\sqrt{\varepsilon_p\omega_0}$, and the optical phonons, being polarized in the direction perpendicular to the chain, are approximated as independent Einstein oscillators with bare frequency ω_0 ($\hbar=1$). Physically, this model was proposed to mimic the interaction of doped holes with apical oxygens in the high-T_c's, e.g., in $YBa_2Cu_3O_{6+x}$, where one can assume that the coupling is not screened because of a low c-axis conductivity and high phonon frequency.[18] Methodically, model (1) represents an extension of the Fröhlich model to a discrete ionic lattice or of the Holstein model including longer ranged EP interactions. Indeed, defining the polaron binding energy as

$$\tilde{\varepsilon}_p=\frac{x_0^2}{\omega_0}\sum_l f_l^2(0)=1.27\varepsilon_p, \tag{3}$$

the Holstein model (HM) results by setting

$$f_l(j)=\kappa\delta_{j,l},$$

$$\tilde{\varepsilon}_p\to\varepsilon_p. \tag{4}$$

Therefore, the model (1) will be subsequently termed the *extended Holstein model* (EHM). In order to parametrize the EP coupling strength for both the HM and EHM we introduce two dimensionless EP coupling constants

$$\lambda=\tilde{\varepsilon}_p/2t,\quad g^2=\tilde{\varepsilon}_p/\omega_0 \tag{5}$$

(in what follows we measure all energies in units of t).

 ©2000 The American Physical Society

So far, analytical and numerical investigations of the EHM have been mainly confined to the determination of the effective mass of the polaron, where it was found that the EHM polaron is much lighter than the small Holstein polaron.[18] First results for the polaron band dispersion and density of states were obtained quite recently, however, the QMC method of calculating the ground-state dispersion used by Kornilovitch[20] is limited to the case where the bandwidth is much smaller than the phonon frequency.

In this paper we present a detailed comparative study of the Holstein and extended Holstein models in order to discuss the effects of long-range EP forces on the lattice polaron formation. Using exact Lanczos diagonalization supplemented by a well-controlled phonon Hilbert space truncation method, we calculate for the first time spectral (optical) properties of the EHM polaron. As stated above such a numerical investigation is especially valuable in the nonadiabatic intermediate-to-strong-coupling transition region, where the electronic and phononic energy scales are not well separated, i.e., $\lambda \simeq \omega_0/t \simeq 1$. In the weak- and strong-coupling regimes the numerical work is supplemented by analytical approaches outlined in the Appendix.

II. QUASIPARTICLE PROPERTIES OF LATTICE POLARONS

A. Numerical methods

Before we discuss the various physical quantities let us briefly sketch our computational scheme. Diagonalizing the coupled EP system (1) on finite 1D lattices with periodic boundary conditions (PBC's), a general K-symmetrized state is given as $|\Psi_K\rangle = \Sigma_{m=0}^{M} \Sigma_{\bar{s}=1}^{\bar{S}(m)} c_K^{m,\bar{s}} |K;m,\bar{s}\rangle$, where $\bar{S}(m) = (N-1+m)!/(N-1)!m!$. K denotes the total momentum of the coupled EP system. Because the phonon Hilbert space has infinite dimension we apply a truncation procedure restricting ourselves to phononic states

$$|m,\bar{s}\rangle_{ph} = \prod_{l=0}^{N-1} \frac{1}{\sqrt{n_l^{\bar{s}}!}} (b_l^{\dagger})^{n_l^{\bar{s}}} |0\rangle_{ph}$$

with at most M phonons, whereby $m = \Sigma_{l=0}^{N-1} n_l^{\bar{s}} \leq M$, and $n_l^{\bar{s}} \in [0,m]$ (cf. Ref. 21). The ground state $|\Psi_{0,K=0}\rangle$ and all excited states $|\Psi_{n,K}\rangle$ contain components that correspond to m-phonon states in the tensorial product Hilbert space of electronic and phononic states. Accordingly,

$$|c_0^m|^2(M) = \sum_{\bar{s}}^{\bar{S}(m)} |c_{K=0}^{m,\bar{s}}|^2 \tag{6}$$

can be taken as a measure of the weight of the m-phonon state in the $K=0$ ground state. In our ED analysis convergence is assumed to be achieved if the ground-state energy $E_0(M)$ is determined with a relative error less than 10^{-7} and $|c_0^M|^2(M) \leq 10^{-7}$. Afterwards static correlation functions can be obtained easily by calculating ground-state expectation values $\langle \Psi_0(M)| \ldots |\Psi_0(M)\rangle$. The numerical computation of dynamical properties, i.e., of spectral functions

$$A^{\mathcal{O}}(\omega) = -\lim_{\varepsilon \to 0^+} \frac{1}{\pi} \mathrm{Im} \left[\left\langle \Psi_0 \middle| \mathbf{O}^{\dagger} \frac{1}{\omega - \mathbf{H} + E_0 + i\varepsilon} \mathbf{O} \middle| \Psi_0 \right\rangle \right]$$
$$= \sum_{n=0}^{D-1} |\langle \Psi_n | \mathbf{O}^{\dagger} | \Psi_0 \rangle|^2 \delta[\omega - (E_n - E_0)], \tag{7}$$

is much more involved. Here $\mathbf{O}$ denotes the matrix representation of a certain operator $\mathcal{O}$, and $\mathbf{H}$ is the very large sparse Hamilton matrix, acting in a Hilbert space with fixed momentum, which, for our problem, has a typical total dimension (D) of about $10^8 - 10^9$. Since it is impossible to determine all the eigenvalues (E_n) and eigenstates ($|\Psi_n\rangle$) of such a huge Hamilton matrix we combine kernel (Chebyshev) polynomial expansion and maximum entropy optimization in order to calculate $A^{\mathcal{O}}(\omega)$ in a well-controlled approximation (for more details see Refs. 21 and 22).

B. Electron lattice correlations

In a first step we discuss the different nature of the polaronic states in the HM and EHM in terms of static correlation functions $\langle n_i q_l \rangle$ between the electron position $[i=0]$ and the oscillator displacement $[q_l \propto (b_l^{\dagger} + b_l)]$ at site l,

$$\chi_{0,l} = \langle c_0^{\dagger} c_0 (b_{0+l}^{\dagger} + b_{0+l}) \rangle / \mathcal{N}. \tag{8}$$

$\chi_{0,l}$ indicates the strength of the electron-induced lattice distortion at $i=0$ and its spatial extent,[14,23,17] where $\mathcal{N} = \Sigma_l \langle c_0^{\dagger} c_0 (b_{0+l}^{\dagger} + b_{0+l}) \rangle$ is a normalization constant [note that $\mathcal{N} = 2(\varepsilon_p/\omega_0)\langle c_0^{\dagger} c_0 \rangle$ holds for the HM].

Figure 1 shows the (static) electron-lattice correlation function (8) in the weak- (a) and intermediate-to-strong- (b) EP coupling regimes, where we have chosen an intermediate phonon frequency ($\omega_0 = 1$) in order to include nonadiabatic effects. Clearly for the quantum phonon model (1) the EP interaction gives rise to a ''dressing'' of the charge carrier at any finite λ, g^2. If the EP coupling is weak, however, the amplitude of $\chi_{0,l}$ is small $\forall\ l$ [in particular smaller than the quantum-lattice (zero-point) fluctuations], that means the lattice deformation could not trap the charge carrier and a so-called ''large'' polaron (LP) is formed in both the Holstein and extended Holstein models. Obviously, the situation is entirely different in the strong-coupling region. For the HM the EP correlations are almost local indicating the formation of a ''small'' polaron (SP). On the other hand, as a result of the nonscreened EP interaction, in the EHM the deformation is spread over many lattice sites, i.e., we found again a LP. It is worthwhile to point out, however, that the electron and the phonon cloud are tightly bound. That means the LP of the EHM as a whole behaves as a well-defined polaronic quasiparticle (cf. Sec. II C) and, in our opinion, it is not possible to discuss the size of the electronic wave function and the size of the lattice distortion separately.[18]

In the insets of Fig. 1 we show the differences between the phonon distribution functions in the weak- and strong-coupling cases, where the ground state is basically a zero-phonon and multiphonon state, respectively. With regard to the discussion of the effective mass in Sec. II E we would like to annotate here, that at small (large) λ the EHM polaron contains more (less) phonons in its phonon cloud than the HM polaron. Of course, in the extreme strong-coupling limit,

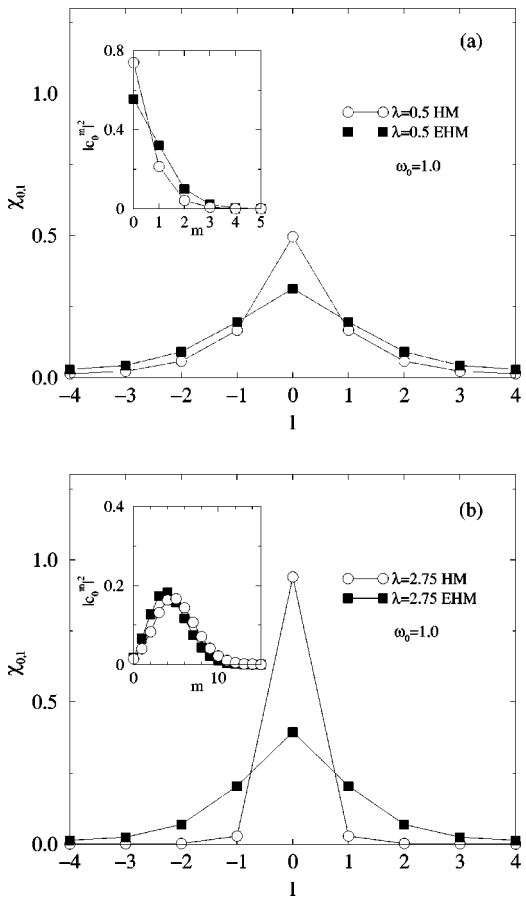

FIG. 1. Electron-lattice correlations in the weak- (a) and strong-coupling (b) cases. ED results are obtained for a finite chain with $N=8$ sites and at most 24 phonons. The insets show the weight of the m-phonon state in the ground state.

the usual Poisson distribution with parameter g^2 results, demonstrating that adjusting the parameters of both models according to Eqs. (3)–(5) is correct.

C. Single-particle spectral function

Next, in order to examine dynamical quasiparticle properties of the HM and EHM polarons, we have evaluated the wave-vector-resolved spectral density function

$$A_K(E)=\sum_n |\langle \Psi_{n,K}|c_K^\dagger|0\rangle|^2 \delta(E-E_{n,K}). \tag{9}$$

The results are presented in Fig. 2. To visualize the spectral weights of the various excitations, the integrated density of states,

$$N_K(E)=\int_{-\infty}^{E} dE' A_K(E'), \tag{10}$$

is also displayed. The weight of the first δ-function peak in each K sector gives the wave-function renormalization factor[24]

$$Z_K=|\langle \Psi_{0,K}|c_K^\dagger|0\rangle|^2, \tag{11}$$

where $|\Psi_{0,K}\rangle$ denotes the single-polaron state with momentum K being lowest in energy. $Z_{K=0}$ is usually termed the

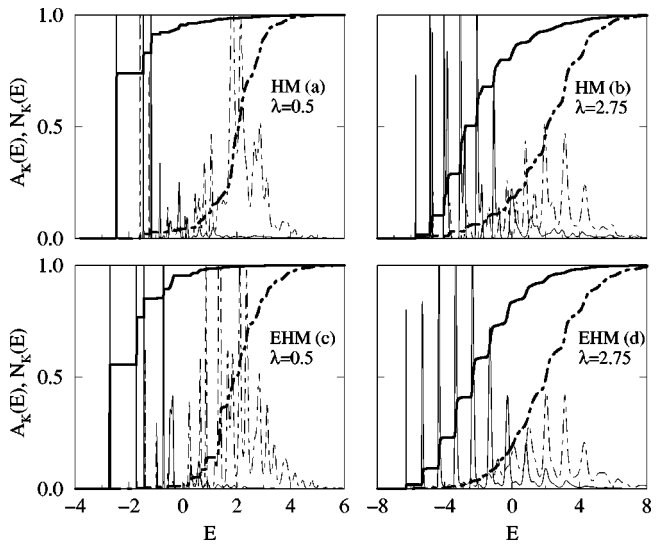

FIG. 2. Single-particle spectral function $A_K(E)$ (thin lines) and partial integrated density of states $N_K(E)$ (thick lines) for the 1D HM (a),(b) and EHM (c),(d) with $\omega_0=1.0$ ($N=8$, $M=24$). Solid and dot-dashed lines belong to states with total momentum $K=0$ and $K=\pi$, respectively.

''quasiparticle-weight factor.'' Since the total integrated area under the entire spectra is unity, the renormalization factor is less than unity and, in particular, $Z_{K=0}$ is a measure how much the polaronic quasiparticle ''deviates'' from the free electron ($Z_{K=0}=1$). In accordance with the discussion in the preceding section, in the weakly interacting EHM we found a stronger dressing of the electron by phonons than in the HM, i.e., a larger renormalization $Z_{K=0}^{\mathrm{EHM}}<Z_{K=0}^{\mathrm{HM}}$. This finding is corroborated by the the weak-coupling theory (WCT) outlined in the Appendix. Table I demonstrates the good agreement of the theoretical approach, working for the infinite system, and finite-cluster diagonalizations, provided that both λ and g^2 are small. Contrary to $Z_{K=0}$, which is only slightly reduced from the free-electron value, the wave-function renormalization factor $Z_{K=\pi}$ is almost zero. The WCT shows that the state with $K=\pi$, being energetically separated by ω_0 from the ground-state energy, is predominantly a phononic state. At strong EP coupling the polaronic band is characterized by $Z_K \ll 1$ $\forall K$, indicating a strong mixing of electronic and phononic degrees of freedom. Calculating the polaronic quasiparticle weight factor within the framework of the strong-coupling theory (SCT) developed in the Appendix [Eq. (A28)] gives $Z_{K=0}$ values which are by a factor of 3 too small as compared to the exact data of Figs. 2(b) and 2(d). The differences mainly arise because these parameters correspond rather to the intermediate-to-strong than to the extreme strong-coupling regime. The qualitative

TABLE I. Quasiparticle weight $Z_{K=0}$ obtained from ED ($N=8$, $M=24$) and within WCT according to Eq. (A7).

	$\lambda=0.1$, $g^2=0.2$		$\lambda=0.5$, $g^2=1/3$	
	ED	WCT	ED	WCT
HM	0.955	0.946	0.893	0.848
EHM	0.918	0.893	0.857	0.781

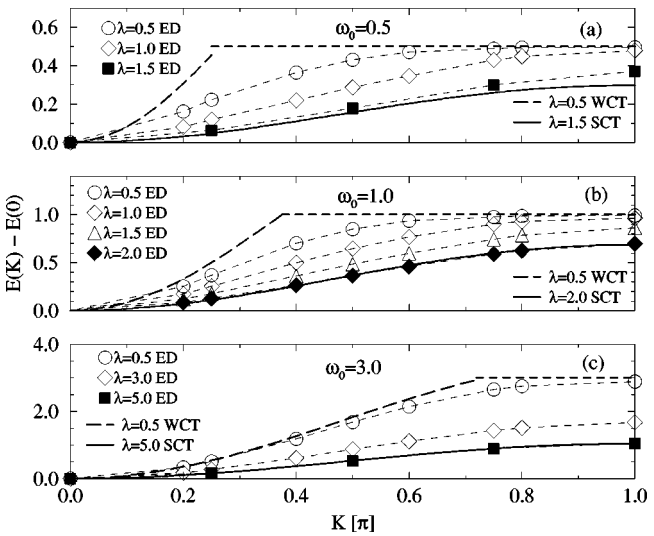

FIG. 3. Band dispersion of the 1D extended Holstein model for low (a), intermediate (b), and high (c) phonon frequencies. Exact data are extracted from finite-lattice diagonalizations with $N=8$ and 10 sites. In the weak- and strong-coupling regimes ED results are compared with the theoretical predictions.

behavior of the single-particle spectral function $A_K(E)$, however, is correctly reproduced by SCT (A27), which yields, above the quasiparticle pole, a sequence of excitations separated by ω_0. Apparently the spectral weight of this incoherent part increases with increasing EP interaction strength.

D. Polaron band structure

Now the so-called ''coherent'' band dispersion, E_K, can be derived from the first peak of $A_K(E)$. Figure 3 compares the dispersion of the energy bands for the EHM at different EP interactions, corresponding to the weak-, intermediate-, and strong-coupling case, where, by going from (a) to (c), ω_0 is increased modeling the adiabatic, intermediate, and antiadiabatic regimes.

Starting with the adiabatic weak-coupling case [Fig. 3(a)], we found that the band structure is nearly unaffected at small momentum, i.e., in the vicinity of the band center. In this region $|\Psi_{0,K}\rangle$ is a quasi-zero-phonon state.[10,26] A different behavior is observed near the zone boundary. Here the band structure is flattened. Such a ''flattening'' has been found for the HM as well and can be attributed to the intersection of the dispersionsless optical phonon branch with the bare electronic cosine band[25,9,10,26] (cf. also Fig. 4). The weak-coupling calculation of E_K [Appendix; Eq. (A6)] reflects this behavior. For the HM, e.g., the correction to ξ_K is given by the integral $\mathcal{I}^{(1)}(K,0)$, which is nonzero only for $(E_K-\omega_0)^2>4t^2$. The latter condition yields a threshold K^*, at which the solution of Eq. (A6) jumps to the bare band dispersion ξ_K. For $K>K^*$, the first excitation in $A_K(E)$ is related to a one-phonon absorption process and as a result the WCT approximation for E_K breaks down. Thus, above K^*, the physical solution is given to lowest order by the dashed line at $E_0+\omega_0$.

The flattening considerably weakens and ultimately vanishes if the EP coupling λ increases. This tendency is especially pronounced for the EHM in the nonadiabatic regime.

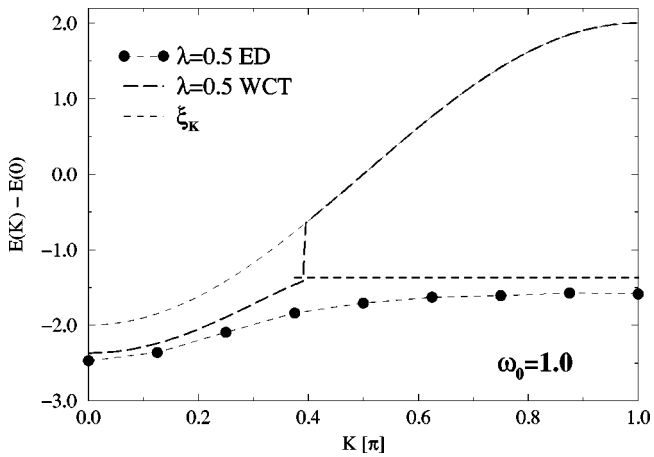

FIG. 4. Flattening of the polaron band dispersion in the 1D Holstein model (weak-coupling case). Long- and short-dashed curves denote the solution of Eq. (A6) and the bare phonon frequency $\omega_0=1.0$, respectively. The agreement of ED and WCT gets better as λ decreases.

As can be seen from Figs. 3(b) and 3(c), in the strong-coupling nonadiabatic regime our SCT yields excellent results. Most notably we do not observe the same drastic polaronic band collapse as in the HM,[10,11] i.e., in the EHM the coherent bandwidth $\Delta E=E_\pi-E_0$ becomes much less renormalized by the EP interaction (e.g., for the HM with $\lambda=5.0$ and $\omega_0=3.0$, we found $\Delta E=0.153$ 19).

E. Effective mass

Another important question is the change in the polaron effective mass induced by the EP coupling. In general it is difficult to compute the mass enhancement, which is defined as an inverse second derivative of the band energy with respect to quasimomentum at the band minimum, $m^*/m \propto[\partial^2 E(K)/\partial K^2|_{K=0}]^{-1}$, using finite-lattice diagonalizations, because $E(K)$ is known at multiples of $2\pi/N$ only rather than at any K, making the limiting procedure $K\to 0$ ill posed. On the other hand, the mass enhancement factor m^*/m is also related to the quasiparticle weight factor $Z_{K=0}$.[24] For the HM, we are able to prove the relation

$$m/m^*_{\mathrm{HM}}=Z^{\mathrm{HM}}_{K=0} \tag{12}$$

in the weak-coupling limit [see the Appendix, Eqs. (A7)–(A9)], i.e., at $\lambda\ll 1$ the polaron effective mass can be read off from the first step in the integrated spectral weight function depicted in Fig. 2. Plotting $Z^{\mathrm{HM}}_{K=0}$ as a function of λ in Fig. 5 and comparing the effective mass determined in this way with the QMC masses, obtained from $m/m^*=\partial^2 E_K/\partial K^2$ without any systematic finite-size errors,[27,18,20] the (perhaps) surprising finding is that Eq. (12) holds for the *whole* coupling region. That means, in the Holstein model, we can determine the effective polaron mass simply by calculating the quasiparticle weight factor. In previous ED studies of the Holstein polaron problem this fact has been ignored so far.

Unfortunately no such simple relation exists for the EHM. This is shown more explicitly in the Appendix, where approximative expressions for m/m^* were derived in the weak- and strong-coupling limits. Note that our analytical weak- and strong-coupling approaches confirm the unexpected non-

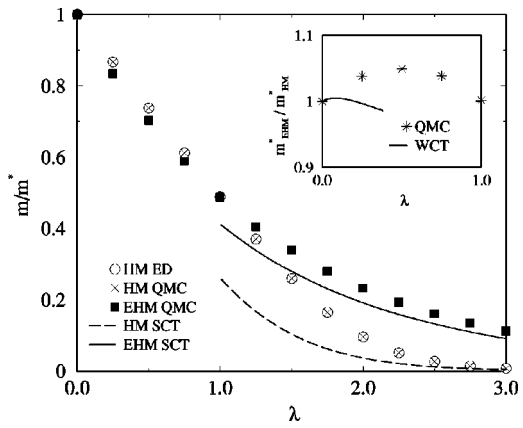

FIG. 5. Inverse effective polaron mass for the 1D (extended) Holstein model at $\omega_0=1.0$. The QMC data are taken from Ref. 18. The ratio of the effective masses of the EHM and HM polarons are displaced in the inset.

monotonic dependence on λ of $m^*_{\mathrm{EHM}}/m^*_{\mathrm{HM}}$, which was found numerically by Alexandrov and Kornilovitch[18] (see inset). In the light of the results presented in the previous sections, it becomes clear that at small EP couplings the EHM LP has to drag a larger phonon cloud coherently through the lattice than the HM LP and therefore acquires a larger effective mass. Further numerical data show that this effect becomes negligible in the weak-coupling antiadiabatic regime, where the phonons can follow the electron instantaneously (cf. also Fig. 3 of Ref. 18). As a matter of course, in the strong-coupling limit the EHM LP is much lighter than the HM SP due to the weaker band renormalization caused by the extended form of the lattice distortion.

F. Optical conductivity

In this section we compare the optical response of HM and EHM polarons. The real part of the optical conductivity,

$$\mathrm{Re}\,\sigma(\omega)=\mathcal{D}\delta(\omega)+\sigma^{reg}(\omega), \tag{13}$$

can be decomposed into the Drude term ($\propto\mathcal{D}$) at $\omega=0$ and a regular contribution for $\omega>0$, which, in linear-response theory, for the (extended) Holstein model is given by

$$\sigma^{reg}(\omega)=\frac{\sigma_0}{N}\sum_{n\neq 0}\frac{\left|\left\langle\Psi_0\left|it\sum_j\left(c_j^\dagger c_{j+1}-c_{j+1}^\dagger c_j\right)\right|\Psi_n\right\rangle\right|^2}{E_n-E_0}\times\delta[\omega-(E_n-E_0)] \tag{14}$$

with $\sigma_0=\pi e^2$ ($T=0$, $K=0$ sector). Again we introduce a ω-integrated spectral weight function,

$$\mathcal{S}^{reg}(\omega)=\int_0^\omega d\omega'\,\sigma^{reg}(\omega'), \tag{15}$$

in order to visualize the intensity of the various excitations more clearly.

Figure 6 shows the optical conductivity obtained at $\omega_0=1.0$ for the HM and EHM on an eight-site lattice using PBC. For the 1D HM the optical absorption spectrum has been discussed in detail in previous work.[23] If the energy to excite one phonon lies inside the bare tight-binding band we found, at weak EP coupling, the first transitions by adding phonons with opposite momentum to only slightly renormalized electronic states (in order to reach the $K=0$ sector of the ground state). However, since the ground state is approximately a zero-phonon state [cf. inset of Fig. 1(a)], the spectral weight of optical transitions involving larger number of phonons is reduced drastically. Of course, the absorption threshold is ω_0 for the infinite system; the shift observed in Fig. 6(a) simply results from the discrete K mesh of our finite system. The situation changes by increasing the EP coupling when in the HM the SP formation takes place. Now the phonon distribution function in the ground state is broadened and in the optical response the overlap with excited multiphonon states is enlarged. As a result the famous SP absorption maximum develops around $\omega\simeq 4\lambda=2\tilde{\varepsilon}_p$ for large couplings.

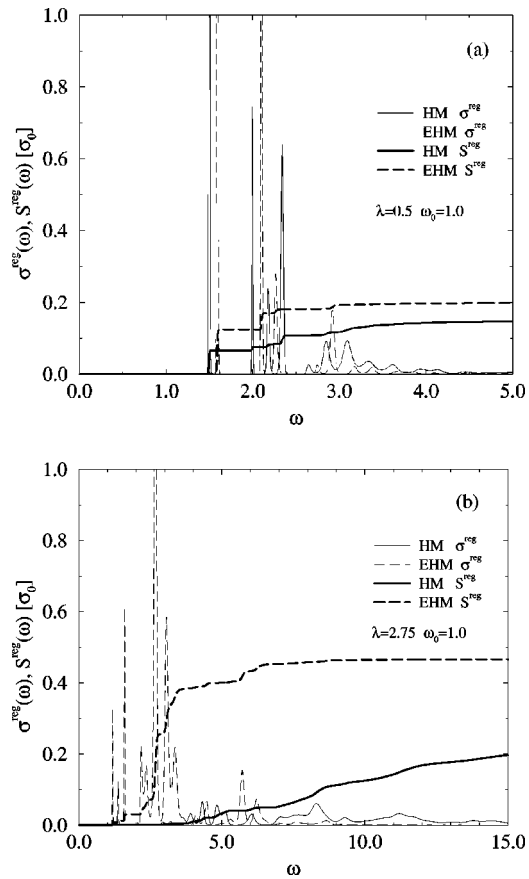

FIG. 6. Optical absorption in the 1D Holstein and extended Holstein models. The regular part of the conductivity σ^{reg} (thin lines) and integrated spectral weight $\mathcal{S}^{reg}$ (thick lines) are shown in the weak- (a) and strong-coupling (b) regimes.

Let us now discuss the optical response in the EHM. Of course, there is little change in the weak-coupling region. At large EP coupling, however, the optical absorption points toward a completely different nature of the polaronic states in the Holstein and extended Holstein models. The EHM polaron clearly shows all the LP signatures but compared to the weak-coupling case and, what is more important, also compared to the HM SP, the optical conductivity is strongly enhanced by multiphonon absorptions processes. The physical reason lies in the nonscreened EP interaction leading to

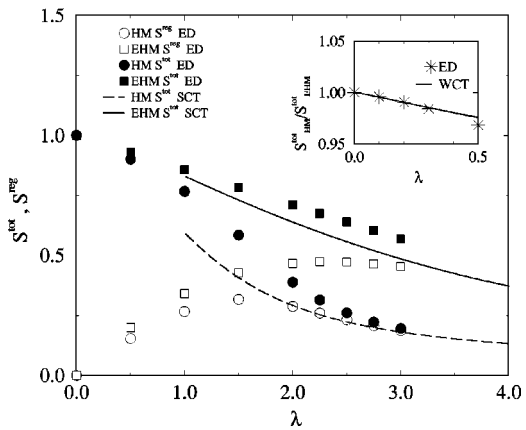

FIG. 7. Renormalized kinetic energy (S^{tot}) and contribution of σ^{reg} to the *f*-sum rule (S^{reg}) as a function of EP coupling (λ) at $\omega_0 = 1.0$.

the form of the lattice distortion depicted in Fig. 1(b). Taking into account the internal structure of the EHM LP it is obvious that the lattice distortion undergoes less relative changes when the charge carrier hops incoherently to neighboring sites accompanied by phonon absorption or emission.[18]

G. Kinetic energy

Integrating Eq. (13) with respect to ω, the familiar *f*-sum rule

$$-\frac{E_{kin}}{2} = \frac{\mathcal{S}^{tot}}{\sigma_0} = \frac{\mathcal{D}}{2\sigma_0} + \frac{\mathcal{S}^{reg}}{\sigma_0}, \tag{16}$$

can be derived, where $\mathcal{S}^{reg} = \mathcal{S}^{reg}(\infty)$. Equation (16) relates optical response and kinetic energy. E_{kin} measures the mobility of the charge carrier.

To elucidate the different nature of HM and EHM polarons in more detail, in Fig. 7 we have displayed the kinetic energy ($\propto \mathcal{S}^{tot}$), renormalized to its value at $\lambda = 0$, together with $\mathcal{S}^{reg}$. Since the kinetic energy contains contributions from both ''coherent'' ($\propto \mathcal{D}$) and ''incoherent'' ($\propto \mathcal{S}^{reg}$) hopping processes, the Drude part can be directly read off from the difference between the filled and open symbols at fixed λ. In agreement with previous numerical results, in the HM we found a continuous transition from a LP to a less mobile SP as the EP interacting increases.[12,23,14] The decrease of S^{tot} in the crossover region, being much more pronounced in the adiabatic regime[23] (as well as for higher dimensions[12,11]), is driven by the sharp drop of the Drude weight.[28] By contrast, in the EHM the kinetic energy decreases very gradually with increasing λ and we observe a substantial Drude contribution even at large EP couplings. This is in accord with the moderate renormalization of the polaronic bandwidth and the minor effective mass (cf. Sec. II D and Sec. II E). In addition, as already stressed in Sec. II E, the optical absorption due to inelastic scattering processes, described by the regular part of the optical conductivity, gives a large contribution. This can be easily understood within second-order perturbation theory (note that one has to go beyond the lowest order of approximation to obtain reliable results for the kinetic energy;[29,9,11] cf. the Appendix): during a second-order hopping process of the EHM LP the lattice distortion of the intermediate state with the charge carrier on a nearest-neighbor site of the initial site fits much better to the polaronic quasiparticle than in the case of the HM SP. The difference between the numerical and theoretical results at larger EP couplings originates from the neglect of longer-ranged hopping processes in our theoretical approach. Of course, such transitions are much more important in the EHM. In addition, let us emphasize that $S^{tot}_{\mathrm{EHM}} > S^{tot}_{\mathrm{HM}}$ holds also in the weak-coupling limit (see inset). That means the stronger reduction of the coherent Drude part, corresponding to the stronger mass enhancement in the weakly-coupled EHM ($m^*_{\mathrm{EHM}}/m^*_{\mathrm{HM}} > 1$, cf. inset Fig. 5), is overcompensated by the incoherent part.

III. CONCLUSIONS

In summary, we have performed an extensive comparative numerical study of polaron formation in the Holstein and extended Holstein models, supplemented by a theoretical analysis of the weak- and strong-coupling limits. The emphasis was on the new effects induced by a nonscreened electron-phonon interaction. The main characteristics of the new polaronic state formed in the EHM are the following.

(i) By its nature the EHM polaron is a large polaron in the whole EP coupling region. That is, the lattice distortion is spread over large distances even if the EP is extremely strong, In this regime a small polaron is formed in the Holstein model.

(ii) For strong EP interactions the EHM polaron propagates in a relatively weakly renormalized band as compared to the HM. Accordingly the effective mass of the large EHM polaron is much smaller than that of the small Holstein polaron with the same polaron binding energy.

(iii) A surprise finding is that the effective mass of the EHM polaron, describing a ''coherent'' band motion, is larger than the effective mass of the HM polaron at weak EP couplings, in particular in the adiabatic case. We have seen that this effect can be attributed to the larger number of phonons the charge carrier has to drag through the lattice if the weak EP interaction is nonscreened.

(iv) From the calculation of the *K*-resolved single-particle spectral function a wave-vector renormalization factor Z_K can be extracted, which indicates, in accordance with (i) and (ii), at weak (strong) EP couplings a stronger (weaker) renormalization of the band states in the EHM than in the HM.

(v) While in the HM the inverse polaron effective mass is directly given by the quasiparticle weight factor, $Z_{K=0}$, the relation is more complicated for the EHM. In the weak-coupling limit this has been corroborated analytically.

(vi) The EHM polaron band dispersion is noncosine for model parameters corresponding to the (adiabatic) weak-to-intermediate coupling regime. In particular, in the weakly coupled EHM, a flattening of the band structure at the zone boundary is definitely observed just as in the HM, but the effect is much less pronounced. Furthermore the flattening rapidly vanishes with increasing EP coupling strength and phonon frequency. In the strong-coupling limit, the EHM exhibits a free-particle-like band dispersion with a bandwidth which, although renormalized, is approximately one or two orders of magnitudes larger than in the HM.

(vii) While in the HM the transition from large to small

polarons is accompanied by significant changes in the optical response, the optical absorption in the EHM shows large polaron characteristics for all EP interaction strengths. Most notably the extended form of the the lattice distortion in the EHM gives rise to a large amount of ''incoherent'' hopping processes contributing to the regular part of the optical conductivity. As a result the regular contribution to the *f*-sum rule is always bigger than in the HM.

(viii) If one takes the averaged kinetic energy as a measure for the mobility of a charge carrier, the EHM polaron is more mobile than the HM polaron, independently of the magnitude of the EP coupling strength. In particular the dramatic kinetic energy loss during the self-trapping transition of the Holstein small polaron is absent in the EHM. On the contrary, one observes a very gradual decrease of the kinetic energy with increasing EP interaction and a substantial Drude contribution even for large EP couplings.

Finally, we would like to stress that the above properties of the EHM large polaron are generic and not an artifact of our 1D system. The relative mass enhancement $m^*_{\mathrm{EHM}}/m^*_{\mathrm{HM}}$ at weak EP interactions, e.g., seems to be even more pronounced in 2D.[18]

ACKNOWLEDGMENTS

The authors are greately indebted to A. S. Alexandrov, H. Büttner, P. Kornilovitch, and A. Weiße for stimulating discussions and, in particular, to P. Kornilovitch for putting his QMC data at our disposal. Numerical calculations were performed at the LRZ München, NIC Jülich, and the HLR Stuttgart. This work was supported by the Deutsche Forschungsgemeinschaft and the Czech Academy of Sciences under Grant No. 436 TSE 113/33.

APPENDIX: ANALYTICAL APPROACHES

Following the previous consideration of the HM,[11] the Hamiltonian for treating the EHM at any λ may be written as

$$\mathcal{H}=-\eta\sum_j c_j^\dagger c_j-\sum_{j,j'}\mathcal{C}_{j'j}c_{j'}^\dagger c_j+\omega_0\sum_l\left(b_l^\dagger b_l+\frac{1}{2}\right), \tag{A1}$$

where η is a c number and $\mathcal{C}_{j'j}$ are generally functions of the phonon operators $b_l^\dagger$, b_l. Using the formalism of generalized Matsubara Green's functions, the polaron self-energy Σ corresponding to Eq. (A1) in the second step of iteration is given by

$$\Sigma(j_1\tau_1;j_2\tau_2)=-\langle\mathcal{C}_{j_1j_2}\rangle\delta(\tau_1-\tau_2)+\sum_{j'j''}\mathcal{G}(j'\tau_1;j''\tau_2)\times[\langle\mathcal{T}_\tau\mathcal{C}_{j_1j'}(\tau_1)\mathcal{C}_{j''j_2}(\tau_2)\rangle-\langle\mathcal{C}_{j_1j'}\rangle\langle\mathcal{C}_{j''j_2}\rangle], \tag{A2}$$

where $\mathcal{G}(j'\tau_1;j''\tau_2)$ means the polaron Green's function in the first approximation (see Refs. 30–32 for details). In the subsequent calculations, the latter equation will be taken as a starting point for the treatment of EHM in the weak- ($\lambda\ll1$) and strong- ($\lambda\gg1$) coupling regimes; in addition, the low-temperature approximation (LTA) defined by $\beta\omega_0\gg1$, and the small carrier-concentration limit ($x\to0$) will be assumed.

1. Weak-coupling regime

In this case, the functions $\mathcal{C}_{j'j}$ are defined by the first and third terms of the Hamiltonian (1), and η is put equal to the chemical potential μ. Applying the Fourier transformation to both sides of Eq. (A2) and carrying out the standard summation over the phonon Matsubara frequencies,[24,11] the polaron self-energy

$$\Sigma_K(\bar\omega)=\xi_K+\omega_0\sum_{d=-\infty}^{\infty}\tilde\varepsilon_p(d)\cos(Kd)\times\int_{-\pi}^{\pi}\frac{dK'}{2\pi}\frac{\cos(K'd)}{\bar\omega+\mu-\omega_0-\xi_{K'}} \tag{A3}$$

is obtained after analytical continuation to the real frequencies ω under assumption of LTA and small x. In writing Eq. (A3), the definition

$$\tilde\varepsilon_p(d)=\tilde\varepsilon_p\sum_l f_l(0)f_l(d)/\sum_l f_l^2(0), \tag{A4}$$

$\xi_K=-2t\cos K$, and $\bar\omega=\omega+i0^+$ were used. The HM limit results from Eq. (A3) by setting

$$\tilde\varepsilon_p(d)=\varepsilon_p\delta_{d,0}. \tag{A5}$$

In view of Eq. (A3), the *polaron band energies* E_K are solutions of the following equation:

$$E_K=\xi_K+\omega_0\sum_{d=-\infty}^{\infty}\tilde\varepsilon_p(d)\cos(Kd)\mathcal{I}^{(1)}(K,d), \tag{A6}$$

and the *renormalization factor of the spectral function*,[24] $Z_K=[1-(\partial/\partial\omega)\mathrm{Re}\,\Sigma_K(\omega)]^{-1}_{\omega=E_K-\mu}$, is determined by

$$Z_K^{-1}=1+\omega_0\sum_{d=-\infty}^{\infty}\tilde\varepsilon_p(d)\cos(Kd)\mathcal{I}^{(2)}(K,d), \tag{A7}$$

where

$$\mathcal{I}^{(n)}(K,d)=\int_{-\pi}^{\pi}\frac{dK'}{2\pi}\frac{\cos(K'd)}{(E_K-\omega_0-\xi_{K'})^n}. \tag{A8}$$

The relation between the *effective polaron mass* m^* and the bare electron mass m [being equal to $(2t)^{-1}$ in 1D] is deduced according to $m/m^*=[\partial E_K/\partial\varepsilon_K]|_{\varepsilon_K\to0}$ with $\varepsilon_K=tK^2$:[24]

$$\frac{m}{m^*}=Z_{K=0}\left[1-\frac{\omega_0}{2t}\sum_{d=-\infty}^{\infty}\tilde\varepsilon_p(d)d^2\mathcal{I}^{(1)}(0,d)\right]. \tag{A9}$$

Note that only for the Holstein model ($d=0$) the effective mass is given by the inverse spectral weight factor $m^*_{\mathrm{HM}}/m=(Z^{\mathrm{HM}}_{K=0})^{-1}$. Using Eq. (A6), the *polaron kinetic energy* results from the relation $E_{kin}=t\partial_tE_K|_{K\to0}$ as

$$E_{kin}=-2tZ_{K=0}\Bigg[1+\omega_0\sum_{d=-\infty}^{\infty}\tilde{\varepsilon}_p(d)\times\int_{-\pi}^{\pi}\frac{dK'}{2\pi}\frac{\cos K'\cos(K'd)}{(E_0-\omega_0-\xi_{K'})^2}\Bigg]. \quad \text{(A10)}$$

2. Strong-coupling regime

In order to generalize the strong-coupling approach, developed in Ref. 11 for the HM, to the EHM case, the long-range interaction of Hamiltonian (1) is eliminated by a non-local Lang-Firsov transformation

$$\mathcal{U}=\prod_l \exp\left\{\frac{x_0}{\omega_0}\sum_j f_l(j)c_j^{\dagger}c_j(b_l^{\dagger}-b_l)\right\}. \quad \text{(A11)}$$

Clearly, the theory based on Eq. (A11) turns into the theory for the HM if the condition (4) is inserted. The canonical transformation (A11) applied to Eq. (1) leads to the polaron binding energy (3) and to the emergence of the multiphonon processes connected with the electron hopping from the site j to the nearest-neighbor sites $j+h$ (h being the elementary translation in units of the lattice constant).

Treating the dynamical EP interaction of the transformed Hamiltonian by means of the formalism outlined in Ref. 11, the polaron self-energy represented in the space of Brillouin-zone K vectors and Matsubara frequencies $i\omega_\nu=i(2\nu+1)\pi/\beta$ is obtained to the second order as

$$\Sigma_K(i\omega_\nu)=-t\sum_h\langle\Phi_{j,j+h}\rangle e^{iKh}+\sum_{\substack{j',j''\\ j_2-j_1}} e^{iK(j_2-j_1)}\times\frac{1}{N}\sum_{K',\zeta}e^{iK'(j'-j'')}\frac{1}{\beta}\int_0^{\beta}d\tau e^{i(\omega_\nu-\omega_\zeta)\tau}\times t^2(\langle\Phi_{j_1,j'}(\tau)\Phi_{j'',j_2}(0)\rangle-\langle\Phi_{j_1,j'}\rangle\times\langle\Phi_{j'',j_2}\rangle)\mathcal{G}_{K'}(i\omega_\zeta). \quad \text{(A12)}$$

The multiphonon operator

$$\Phi_{j,j+h}=\exp\left\{\frac{x_0}{\omega_0}\sum_l[f_l(j+h)-f_l(j)](b_l^{\dagger}-b_l)\right\} \quad \text{(A13)}$$

occurring in the transformed hopping term of Eq. (A1) induces the polaron band narrowing in the first order, namely,

$$\tilde{t}\equiv t\langle\Phi_{j,j+h}\rangle=t\exp\{-g^2\Delta(1)\coth(\beta\omega_0/2)\}, \quad \text{(A14)}$$

where

$$\Delta(1)=1-\sum_l f_l(0)f_l(1)/\sum_l f_l^2(0). \quad \text{(A15)}$$

In the LTA $\beta\omega_0\gg1$, we have $\tilde{t}\simeq t\exp\{-g^2\Delta(1)\}$, $\tilde{\xi}_K=-2\tilde{t}\cos K$, and

$$\Sigma_K(i\omega_\nu)=\tilde{\xi}_K+\sum_{\substack{j',j''\\ j_2-j_1}} e^{iK(j_2-j_1)}\frac{1}{N}\sum_{K',\zeta}e^{iK'(j'-j'')}\times\tilde{t}^2\sum_{s\geq1}\frac{\varkappa^s}{s!}\frac{1}{\beta}\frac{2s\omega_0}{(s\omega_0)^2+(\omega_\zeta-\omega_\nu)^2}\mathcal{G}_{K'}(i\omega_\zeta). \quad \text{(A16)}$$

The parameter $\varkappa\equiv\varkappa(d,d_1,d_2)$ is given by

$$\varkappa=\frac{x_0^2}{\omega_0^2}\sum_l f_l(0)[f_l(d)+f_l(d+d_2-d_1)-f_l(d-d_1)-f_l(d+d_2)]. \quad \text{(A17)}$$

Here $d=j_2-j_1$, $d_1=j'-j_1$ and $d_2=j''-j_2$ are elementary translations. The summation over ζ is now evaluated using the lowest-order approximation for the Green's function $\mathcal{G}_K(i\omega_\zeta)$ corresponding to a quasiparticle energy spectrum of the form $\tilde{\xi}_K-\tilde{\varepsilon}_p$. After carrying out this summation in LTA and for small carrier concentration, the wave-vector and frequency-dependent polaron self-energy is obtained from Eq. (A16) by the analytical continuation $i\omega_\nu\to\bar{\omega}$ as

$$\Sigma_K(\bar{\omega})=\tilde{\xi}_K+\tilde{t}^2\sum_{d,d_1,d_2}e^{iKd}\frac{1}{N}\sum_{K'}\times\sum_{s\geq1}\frac{\varkappa^s}{s!}e^{-iK'(d+d_2-d_1)}\frac{1}{\bar{\omega}-\tilde{\xi}_{K'}+\tilde{\varepsilon}_p+\mu-s\omega_0}. \quad \text{(A18)}$$

If we neglect $\tilde{\xi}_{K'}$ on the right-hand side (rhs) of Eq. (A18), in the strong-coupling limit, the *polaron band dispersion* E_K can be easily determined from

$$E_K=\tilde{\xi}_K-2\tilde{t}^2\sum_{s\geq1}\frac{(2g^2\Delta(1))^s}{s!}\frac{1}{s\omega_0-E_K}+\tilde{t}\tilde{\xi}_{2K}\sum_{s\geq1}\frac{[g^2\Delta(2)]^s}{s!}\frac{1}{s\omega_0-E_K}, \quad \text{(A19)}$$

where

$$\Delta(2)=1-\frac{2\sum_l f_l(0)f_l(1)-\sum_l f_l(0)f_l(2)}{\sum_l f_l^2(0)}. \quad \text{(A20)}$$

On the basis of Eq. (A19), the *polaron mass enhancement* can be calculated from

$$m/m^*=e^{-g^2\Delta(1)}[\partial E_K/\partial\tilde{\varepsilon}_K]|_{\tilde{\varepsilon}_K\to0}, \quad \text{(A21)}$$

where $\tilde{\varepsilon}_K=\tilde{t}K^2$. Substituting, for $K\to0$, $\tilde{\xi}_K=-2\tilde{t}+\tilde{\varepsilon}_K$ and $\tilde{t}\tilde{\xi}_{2K}=-2\tilde{t}(\tilde{t}-2\tilde{\varepsilon}_K)$, we find

$$\frac{m}{m^*}=e^{-g^2\Delta(1)}\mathcal{Z}_{E_0}^{-1}\times\left[1+4te^{g^2[\Delta(2)-\Delta(1)]}\left\langle\frac{1}{s\omega_0-E_0}\right\rangle_{g^2\Delta(2)}\right] \tag{A22}$$

with

$$\mathcal{Z}_{E_K}=\left[1+2t^2\left(\left\langle\frac{1}{(s\omega_0-E_K)^2}\right\rangle_{2g^2\Delta(1)}+e^{g^2[\Delta(2)-2\Delta(1)]}\left\langle\frac{1}{(s\omega_0-E_K)^2}\right\rangle_{g^2\Delta(2)}\cos 2K\right)\right]. \tag{A23}$$

Here $\langle\ldots\rangle_\varrho$ denotes the average over $s\geqslant 1$ with respect to the Poisson distribution with the parameter ϱ.

Accordingly, the *polaron kinetic energy* takes the form

$$E_{kin}=-2t\mathcal{Z}_{E_0}^{-1}\left[e^{-g^2\Delta(1)}+2t\left\langle\frac{1}{s\omega_0-E_0}\right\rangle_{2g^2\Delta(1)}+2te^{g^2[\Delta(2)-2\Delta(1)]}\left\langle\frac{1}{s\omega_0-E_0}\right\rangle_{g^2\Delta(2)}\right]. \tag{A24}$$

Finally, in order to discuss qualitatively the behavior of the single-particle spectral function reported in Sec. II C, we calculate $A_K(\omega)$ in the strong-coupling limit. Applying the transformation (A11), the electron operators are transformed into

$$\tilde{c}_j^{(\dagger)}=\exp\left\{(-)\frac{x_0}{\omega_0}\sum_l f_l(j)(b_l^\dagger-b_l)\right\}c_j^\dagger. \tag{A25}$$

Consequently, the spectral function is determined by the imaginary part of the retarded Green's function $\tilde{\mathcal{G}}^R(K,\omega)$ of the operators $\tilde{c}_K$, $\tilde{c}_K^\dagger$. Owing to the relation between the time-ordered products of operators and the retarded Green's functions of the same operators[33] we consider the time-ordered product $\langle\mathcal{T}_t\tilde{c}_K(t)\tilde{c}_K^\dagger(0)\rangle$ and perform a decoupled average over the phonon and charge variables. In the limit $T\to 0$ we get

$$\langle\mathcal{T}_t\tilde{c}_K(t)\tilde{c}_K^\dagger(0)\rangle=e^{-g^2}\left[\langle\mathcal{T}_t c_K(t)c_K^\dagger(0)\rangle+\frac{1}{N}\sum_{K'}\sum_d\sum_{s\geqslant 1}\frac{1}{s!}\left(\frac{\tilde{\varepsilon}_p(d)}{\omega_0}\right)^s\times e^{-is\omega_0 t}e^{i(K-K')d}\times\langle\mathcal{T}_t c_{K'}(t)c_{K'}^\dagger(0)\rangle\right]. \tag{A26}$$

The relation between the imaginary parts of retarded Green's functions $\tilde{\mathcal{G}}^R(K,\omega)$ and $\mathcal{G}^R(K,\omega)$ of operators $\tilde{c}_K$ and c_K, respectively, is obtained from the Fourier transformation of Eq. (A26). As a result, the spectral function

$$\tilde{A}_K(\omega)=-2\,\mathrm{Im}\,\tilde{\mathcal{G}}_K^R(\omega)=e^{-g^2}\mathcal{Z}_{E_K}^{-1}2\pi\delta(\omega-[E_K-\varepsilon_p-\mu])+e^{-g^2}\sum_d\sum_{s\geqslant 1}\frac{1}{N}\sum_{K'}\frac{1}{s!}\left(\frac{\tilde{\varepsilon}_p(d)}{\omega_0}\right)^s\cos[(K-K')d]\times\mathcal{Z}_{E_{K'}}^{-1}2\pi\delta(\omega-[E_{K'}+s\omega_0-\varepsilon_p-\mu]) \tag{A27}$$

is determined by the spectral functions $A_{K'}(\omega-r\omega_0)$ with $r\geqslant 0$ corresponding to $\mathcal{G}_{K'}^R(\omega-r\omega_0)$, i.e., using the self-energy $\Sigma_{K'}(\omega')$ derived in this section. The energies $E_{K'}$ on the rhs of Eq. (A27) are solutions of Eq. (A19) and the factors $\mathcal{Z}_{E_{K'}}$ are given by Eq. (A23). The first term on the rhs of Eq. (A27) describes the quasiparticle of momentum K and the second term, being a sum over the entire polaron band, corresponds to the incoherent part of the spectral function. Inserting the condition (A5) into Eq. (A27), the spectral function of the Holstein model is obtained, which differs by the self-consistently determined $E_{K'}$ and $\mathcal{Z}_{E_{K'}}$ from the result of Alexandrov and Ranninger.[34]

In particular, at $K=0$, $r=0$, the *quasiparticle weight factor* results as

$$Z_{K=0}=e^{-g^2}\mathcal{Z}_{E_0}^{-1}. \tag{A28}$$

Here it is necessary to point out the different level of approximation we used in deriving Eqs. (A22) and (A28). Therefore, it is not possible to verify the HM relation (12) by the above strong-coupling calculation of $Z_{K=0}$. The leading exponential dependence of Eqs. (A22) and (A28), however, is found to be the same (not the same) for the HM (EHM), in good agreement with the numerical results of Figs. 2 and 5.

We recently had a valuable discussion with A. S. Alexandrov and P. Kornilovitch,[35] which forces us to motivate our teminology ''large EHM polaron'' in some more detail in order to avoid confusion of people outside the polaron community. Alexandrov and Kornilovitch used in their study of the model (1) with (2) the notation ''small Fröhlich polaron'' to characterize the polaronic state in the strong-coupling regime,[18] mainly because the polaron mass increases exponentially with coupling as in the standards SP theory, albeit with a somewhat reduced exponent.[35] However, while for the usual 1D HM (1) with (4), there is a one-to-one correspondence between weak-coupling (strong-coupling) situation and LP (SP) formation, the interrelation is more complex in the EHM. Indeed, in the strong-coupling limit of the EHM, the polaronic quasiparticle, consisting of the electron and its concomitant phonon cloud, is definitely *extended* although its mass becomes exponentially large. Thus, following Holstein's[4] distinction between SP and LP according to the spatial extent of the lattice distortion caused by the charge carrier, we specified the polaron in the EHM as ''large'' and used in addition the term ''Holstein'' instead of ''Fröhlich'' to discriminate our ''lattice'' polaron from the ''continuum'' (Fröhlich) polaron. Moreover, besides this rather ''static'' characteristic there is another much more profound ''dy-

namical'' aspect: the well-known SP absorption maximum at $\omega \sim 2\tilde{\varepsilon}_p$ is missing for polarons in the EHM, irrespective of the coupling strength. On the contrary, appreciable phonon-assisted absorption occurs at lower frequencies, owing to the extended lattice deformation, which makes the lattice adaptation during the carrier hopping easier. This clearly demonstrates the different nature of the ''small'' HM polaron and the ''large'' EHm in the large EP interaction limit.

[1] L. D. Landau, Z. Phys. **3**, 664 (1933).
[2] E. K. H. Salje, A. S. Alexandrov, and W. Y. Liang, *Polarons and Bipolarons in High Temperature Superconductors and Related Materials* (Cambridge University Press, Cambridge, 1995).
[3] M. Jaime, H. T. Hardner, M. B. Salamon, M. Rubinstein, P. Dorsey, and D. Emin, Phys. Rev. Lett. **78**, 951 (1997).
[4] T. Holstein, Ann. Phys. (Leipzig) **8**, 325 (1959).
[5] H. Fröhlich, Adv. Phys. **3**, 325 (1954).
[6] J. Ranninger and U. Thibblin, Phys. Rev. B **45**, 7730 (1992).
[7] F. Marsiglio, Phys. Lett. A **180**, 280 (1993).
[8] A. S. Alexandrov, V. V. Kabanov, and D. K. Ray, Phys. Rev. B **49**, 9915 (1994).
[9] W. Stephan, Phys. Rev. B **54**, 8981 (1996).
[10] G. Wellein and H. Fehske, Phys. Rev. B **56**, 4513 (1997).
[11] H. Fehske, J. Loos, and G. Wellein, Z. Phys. B: Condens. Matter **104**, 619 (1997).
[12] H. D. Raedt and A. Lagendijk, Phys. Rev. Lett. **49**, 1522 (1982).
[13] E. Berger, P. Valášek, and W. v. d. Linden, Phys. Rev. B **52**, 4806 (1995).
[14] E. Jeckelmann and S. R. White, Phys. Rev. B **57**, 6376 (1998).
[15] C. Zhang, E. Jeckelmann, and S. R. White, Phys. Rev. B **60**, 14 092 (1999).
[16] A. W. Romero, D. W. Brown, and K. Lindenberg, J. Chem. Phys. **109**, 6504 (1998).
[17] J. Bonča, S. A. Trugman, and I. Batistić, Phys. Rev. B **60**, 1633 (1999).
[18] A. S. Alexandrov and P. E. Kornilovitch, Phys. Rev. Lett. **82**, 807 (1999).
[19] P. E. Kornilovitch, Phys. Rev. Lett. **81**, 5382 (1998).
[20] P. E. Kornilovitch, Phys. Rev. B **60**, 3237 (1999).
[21] B. Bäuml, G. Wellein, and H. Fehske, Phys. Rev. B **58**, 3663 (1998).
[22] R. N. Silver and H. Röder, Phys. Rev. E **56**, 4822 (1997).
[23] G. Wellein and H. Fehske, Phys. Rev. B **58**, 6208 (1998).
[24] G. D. Mahan, *Many-Particle Physics* (Plenum, New York, 1990).
[25] Y. B. Levinson and E. I. Rashba, Rep. Prog. Phys. **36**, 1499 (1973).
[26] J. M. Robin, Phys. Rev. B **58**, 14 335 (1998).
[27] P. E. Kornilovitch and E. R. Pike, Phys. Rev. B **55**, R8634 (1997).
[28] M. Capone, W. Stephan, and M. Grilli, Phys. Rev. B **56**, 4484 (1997).
[29] Y. A. Firsov and E. K. Kudinov, Fiz. Tverd. Tela **39**, 2159 (1997) [Phys. Solid State **32**, 1930 (1997)].
[30] J. Schnakenberg, Z. Phys. **190**, 209 (1966).
[31] J. Loos, Z. Phys. **96**, 149 (1994).
[32] L. P. Kadanoff and G. Baym, *Quantum Statistical Mechanics* (Benjamin-Cumming, Reading, MA 1962).
[33] S. Doinach and E. H. Sondheimer, *Green's Functions for Solid State Physicists* (Benjamin, Reading, 1974).
[34] A. S. Alexandrov and J. Ranninger, Phys. Rev. B **45**, 13 109 (1992).
[35] A. S. Alexandrov and P. Kornilovitch (private communication).